Impact of carbon injection in 4H-SiC on defect formation and minority carrier lifetime

Marianne Etzelmüller Bathen [a,b,*], Robert Karsthof [a], Augustinas Galeckas [a], Piyush Kumar [b], Andrej Yu. Kuznetsov [a], Ulrike Grossner [b], Lasse Vines [a]

[a] *Department of Physics/ Centre for Materials Science and Nanotechnology, University of Oslo, 0316 Oslo, Norway*
[b] *Advanced Power Semiconductor Laboratory, ETH Zürich, Physikstrasse 3, 8092 Zürich, Switzerland*

ARTICLE INFO

ABSTRACT

Point defects in silicon carbide (SiC) can act as charge carrier traps and have a pronounced impact on material properties such as the mobility and carrier lifetime. Prominent among these traps is the carbon vacancy (V_C) with a demonstrated detrimental effect on the minority carrier lifetime in 4H-SiC epitaxial layers. Hence, a variety of methods for V_C removal have been proposed. Common to all is that they involve some sort of C-injection into the epi-layer that leads to annihilation of V_C with C interstitials (C_i) via the reaction $C_i + V_C \rightarrow \emptyset$. However, many studies on injection of C_i for removal of V_C do not take into account the potential effect of any additional defects that are formed as a result of excess C in the material, including electrically active defects that introduce energy levels in the SiC band gap. Herein, we study the formation and impact of carbon related defects that are introduced in 4H-SiC epi-layers by injection of excess carbon. C-injection is achieved by annealing 4H-SiC epi-layers covered by a graphitized photoresist known as a C-cap at 1250 °C for different durations. The resulting appearance of defects in the samples is monitored using deep level transient spectroscopy (DLTS) and minority carrier transient spectroscopy (MCTS) measurements, which reveal the formation of both minority and majority carrier traps as a result of the C-injection. Intriguingly, the injected carbon is also found to interact with a perennially present impurity in 4H-SiC epi-layers and a potentially lifetime limiting defect, namely boron. Furthermore, we monitor the minority carrier lifetime as a function of C-injection time and depth from the surface using cross-sectional time-resolved photoluminescence (TRPL) measurements. Both the defect distributions and the minority carrier lifetime are found to depend strongly on the duration of the C-cap anneal, with a marked depth dependence being present for all samples studied. The moderate temperature C-cap annealing treatment is proposed as a method for enhancing the carrier lifetime in n-type 4H-SiC epi-layers for power device applications.

1. Introduction

Silicon carbide in the 4H polytype (4H-SiC) is a wide bandgap material with excellent resistance to extreme environments including high temperature and high voltage and is showing promise for power electronics applications [1,2]. However, defects are perennially present in 4H SiC epitaxials layers (epi-layers), where they can act as charge carrier traps and alter the electro-optical properties of the material. One sub-class of such defects in SiC are those like the Si vacancy (V_{Si}) and divacancy ($V_{Si}V_C$) that exhibit quantum compatible properties on the macroscopic scale which gives rise to single-photon emission and coherent manipulation of single spins trapped at the defect [3,4]. On the other hand, many of the carrier traps in SiC can have a pronounced

detrimental impact on material properties such as charge carrier lifetime and mobility, and it is this type of defect that is of great import for power device engineering.

The perhaps most prominent point defect in SiC, that is perennially present even in state-of-the-art 4H-SiC epi-layers, is the carbon vacancy (V_C). The V_C is often attributed with limiting the minority carrier lifetime in 4H-SiC epi-layers [5,6] due to the efficient carrier capture of the V_C's trap levels. These include the (2-/0) negative-U acceptor level assigned to the $Z_{1/2}$ peak that is commonly observed in deep level transient spectroscopy (DLTS) measurements of n-type 4H-SiC, and the (2+/+/0) donor level assigned to the $EH_{6/7}$ DLTS peak [7]. The relatively low formation energies of V_C (~4.5 eV–5 eV [8–10]) ensure that the defects can be thermally generated above 1500 °C and V_C are

---

thus formed during epitaxial SiC growth by chemical vapor deposition (CVD). This leads to background concentrations of the V_C in the range of $\sim 5 \times 10^{12}$ cm^{-3} in state-of-the-art 4H-SiC epi-layers [11].

A variety of strategies for V_C removal have been devised to combat its detrimental impact on device performance. Three main strategies for V_C removal have been widely adopted: (i) near-surface ion implantation followed by high temperature annealing [12], (ii) thermal oxidation [13,14], and (iii) annealing at high temperatures with a carbon cap [15]. This C-cap is made of graphitized photoresist and is commonly used to protect the sample from loss of surface atoms and surface roughening during high-temperature processing such as post-implantation annealing for dopant activation [16–18]. The common factor between the three V_C removal methods is that they are all essentially different methods for injecting excess C atoms into the epi-layer. The injected interstitial carbon (C_i) annihilates with V_C according to $C_i + V_C \rightarrow \emptyset$, leading to a reduced V_C density.

Recently, another defect species was shown to have a similar impact on the minority carrier lifetime in as-grown 4H-SiC epi-layers as the $Z_{1/2}$, namely boron related impurities. Boron can substitute for Si or C and introduces two energy levels in the lower half of the 4H-SiC band gap: shallow boron (labeled B) at $E_V + 0.27$ eV and deep boron (the D-center) at $E_V + 0.61$ eV [19], where E_V denotes the valence band edge. The shallow B level has been assigned to B on Si site, B_{Si} [20], while the D-center origin was long debated. The earlier model attributed the D-center to a $B_{Si} - V_C$ complex [20], while more recent studies assign the D-center to B on C site, B_C [21,22]. In a previous work [23] we studied as-grown 4H-SiC epi-layers where the minority carrier lifetime turned out to not be correlated with the presence of $Z_{1/2}$, but rather depended on the presence of the D-center. Thus, any C-injection based treatment to enhance the minority carrier lifetime should consider the impact on boron related defect levels as well.

In the event that the amount of injected carbon during, e.g., a C-cap anneal overshadows that of pre-existing V_C in the epi-layer, the injected carbon itself can cause the formation of new electrically active defects, or interact with other defects that are already present in the as-grown epi-layers. Studies on the defects related to the injected carbon itself, however, and the accompanying effect on material properties such as the carrier lifetime, remain scarce. Thermal oxidation has been shown to generate several electrically active defect levels in SiC that were predicted to be C-related [24], but the full temperature range was not probed and the nature of the defect levels remains uncertain. Furthermore, one cannot exclude the involvement of oxygen during the thermal oxidation process. In a recent study [25] we report on defect levels that appear in the upper portion of the band gap upon using a C-cap as a carbon source and find three electron traps at 0.38 eV ($E_{0.38}$), 0.59 eV ($E_{0.59}$) and 0.7 eV ($E_{0.7}$) below the conduction band edge (E_C) that appear in conjunction with the disappearance of the V_C. The $E_{0.38}$ level exhibits a remarkable instability upon annealing above room temperature, pointing towards an origin related to single C interstitials (C_i). The other two levels ($E_{0.59}$ and $E_{0.7}$) are more stable and are likely caused by carbon related complexes. However, only the temperature range 20 K–300 K was probed, minority carrier traps were not considered, and the impact of the deep levels on material properties such as the carrier lifetime remains unknown.

Herein, we continue the study from Ref. [25] and investigate the impact of injecting excess C into SiC on defect formation and material properties in 150 μm thick 4H-SiC epitaxial layers containing low initial concentrations of V_C and other impurities. To limit the involvement of other point defect species and impurities, the method of choice for the C-injection is annealing at 1250 °C with a graphitized photoresist (C-cap) covering the epi-layer surface and acting as a carbon source. The thermally induced introduction of excess carbon from the capping layer into the SiC is monitored using deep level transient spectroscopy (DLTS) and minority carrier transient spectroscopy (MCTS) to enable mapping of (almost) the entire band gap. The low concentration of other defects prior to and during annealing to a large extent facilitates

the separation of interstitial- and vacancy-related defect levels. Finally, the impact of the C-injection treatment on material properties is investigated using time-resolved photoluminescence (TRPL) spectroscopy in a cross-sectional view, which provides depth-resolved information on the minority carrier lifetime from the surface throughout the entire epi-layer until the substrate.

2. Methodology

Nitrogen doped n-type 4H-SiC (0001) epitaxial layers were used for the carbon injection experiments. The epi-layers have approximately 150 μm thickness as determined by optical and electron microscopy, and a free charge carrier concentration of $\sim 2 \times 10^{14}$ cm^{-3} as determined by capacitance–voltage (CV) measurements. The epi-layers are grown 4° off the *c*-axis (0001) on highly doped ($N_D \sim 8 \times 10^{18}$ cm^{-3}) n-type 4H-SiC substrates and are purchased from Ascatron AB, Sweden. The wafer was diced into 7×7 mm^2 samples and cleaned following a full RCA process to remove contaminants and the native oxide prior to carbon cap formation.

The carbon cap (C-cap) was formed by spin coating the samples with a photoresist (type AR-U 4030) on the front and back sides. The total resist thickness was ~ 5 μm and required multiple spin coating cycles. A heat treatment in an RTP furnace was then performed at 900 °C for 10 min in vacuum ($p = 5 \times 10^{-5}$ mbar) to graphitize the photoresist. To inject carbon atoms from the C-cap into the 4H-SiC, the capped samples were annealed in a tube furnace equipped with Ar atmosphere at 1250 °C for three different durations: 1.5 h, 2.5 h and 6.6 h. The C-cap is typically removed in O_2 ambient at 900 °C. For these samples, out-gassing of oxygen from the ceramic furnace tube resulted in the C-cap having mostly vanished after the anneals. The sample surfaces had not deteriorated significantly after annealing as determined by optical microscopy and electrical measurements. The C-injection experiment is described in further detail in Ref. [25].

After annealing at 1250 °C and removal of any native oxide by a second HF dip, Schottky barrier diodes (SBDs) were formed on the epi-layer surfaces by electron-beam evaporation of Ni through a shadow mask. Semi-transparent Schottky contacts were fabricated to enable probing of minority carrier traps by optical excitation. The lower part of the Schottky contact was 600 μm or 900 μm in diameter with ~ 10 nm thickness, to enable light to penetrate to the space charge region, while the top layer had 300 μm diameter and 100 nm thickness, to enable contacting of the SBD for DLTS and MCTS measurements. The backside Ohmic contact was formed using silver paste.

The electrically active defects that were created by annealing the C-capped samples were characterized using DLTS and MCTS in the 100 K–600 K temperature range. For DLTS, a reverse bias of -5 V was applied to the samples followed by sequential pulses to 0 V with a pulse width of 100 ms. The period width was 200 ms or 50 ms. For the present samples, with doping density of $\sim 2 \times 10^{14}$ cm^{-3}, this translates to a depletion region width (and therefore probing depth during DLTS) of ~ 5.0 μm at -5 V bias voltage. During the MCTS measurements, the samples were kept at a reverse bias of -1 V and an optical pulse of 200 ms was applied using an LED with a wavelength of 365 nm and 200 mW power. The period width was 200 ms. At -1 V reverse bias, the estimated depletion region width is ~ 2.1 μm. For both DLTS and MCTS measurements, a Fourier transform of the recorded transients was performed using up to 28 correlation functions. The DLTS/MCTS signal shown in the following refers to the coefficient of the sine term (b1) in the Fourier series of the deep level or minority carrier transient Fourier spectroscopy (DLTFS/MCTFS) [26]. Cooling was achieved using a closed-cycle He refrigerator. The ramping rate during the DLTS and MCTS measurements was 1 K min^{-1}. All measurements were performed starting at low temperature with a second run following immediately after, starting at high temperature, to reveal any dynamic effects in the defect distributions.
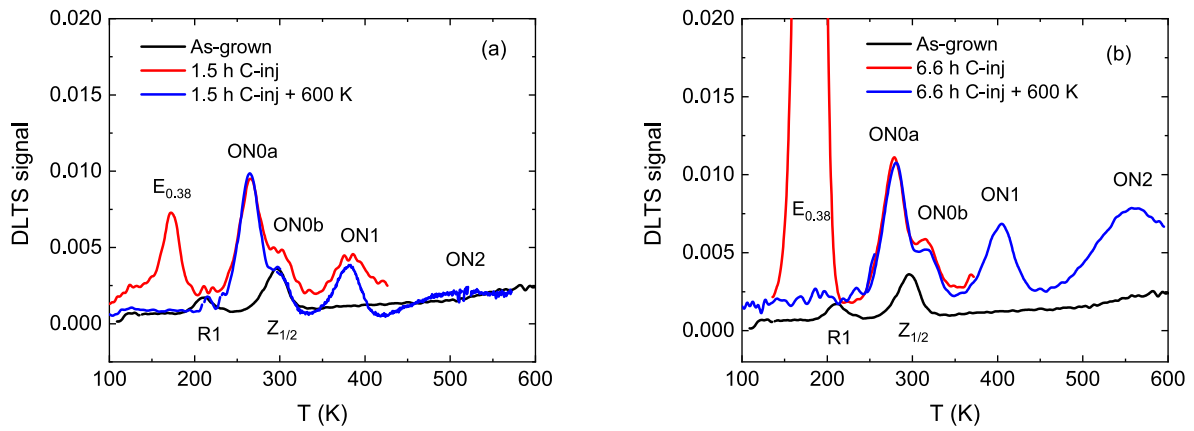
Fig. 1. DLTS spectra showing the effect of C-injection after (a) 1.5 h and (b) 6.6 h annealing with a C-cap. The as-grown sample was probed with DLTS parameters $T_w = 200$ ms, $t_p = 100$ ms and $V_r = -5$ V (black curve). The DLTS parameters for the 1.5 h annealing were $T_w = 200$ ms, $t_p = 100$ ms and $V_r = -5$ V. The DLTS parameters for the 6.6 h annealing were $T_w = 50$ ms, $t_p = 100$ ms and $V_r = -5$ V.

Time-resolved photoluminescence (TRPL) measurements were performed at room temperature (RT) to extract the minority carrier lifetime in the epi-layers at various distances from the surface before and after annealing with the C-cap. TRPL measurements were performed in a cross-sectional view after polishing the sample edge. The depth-resolved carrier lifetime profiling across the epi-substrate stack was realized by employing imaging TRPL spectroscopy in orthogonal pump-probe geometry (ortho-TRPL) [27]. A uniform photo-generation of carriers across the epi-layer was realized by deep-penetrating 372 nm excitation ($\alpha^{-1} > 400\,\mu$m) of a 50 ps pulsed laser (PicoQuant, average power 2 mW at 40 MHz) impinging normally onto the epi-layer surface. The near-band-edge emission from the orthogonal to excitation plane of the sample's cross-section was analyzed by an imaging spectroscopy system comprised of a microscope (50X objective, Mitutoyo) coupled to an imaging spectrograph (HORIBA Jobin Yvon, iHR320) equipped with an EMCCD camera (Andor, iXon888) and a fast PMT detector (Becker&Hickl, PMC100) linked to photon counters (PicoQuant, TC-SPC TimeHarp200 and MCS NanoHarp250). The spatial resolution is determined by the microscope magnification and the width of the region-of-interest (ROI) set by the entrance slits of the imaging spectrograph. In the present study, TRPL signal was collected from a 10 μm wide ROI. The time resolution of the TRPL system is around 50 ps in time-correlated single photon counting (TCSPC) mode upon deconvolution of the system response function. This high resolution is relevant for measuring fast PL decay transients in nanosecond time domain typical to SiC substrate material. For high crystallinity epi-layers exhibiting minority carrier lifetimes in the microsecond range, the TRPL system is operated in multichannel scaling (MCS) photon counting mode, which offers a time resolution of 4 ns.

3. Results

3.1. Majority carrier traps

Fig. 1 shows the electrically active defect levels that are introduced in the upper half of the 4H-SiC band gap by annealing with a C-cap for (a) 1.5 h and (b) 6.6 h as measured by DLTS. Two distinct defect levels are observed in the as-grown sample in the 100 K–600 K temperature range prior to C-injection (black curve): The $Z_{1/2}$ level assigned to the double acceptor (0/2-) negative-U transition of the V_C [7], and a level labeled R1 at 0.41 eV below the conduction band edge (E_C). Table 1 summarizes the trap parameters for the majority carrier traps depicted in Fig. 1. We note that the level labeled R1 observed in the as-grown sample shares energy level position with the S1 defect, however, as S2 was not simultaneously observed, R1 is likely not related to the S-center [28,29].

As previously shown in Ref. [25], the $Z_{1/2}$ level assigned to $V_C(0/2-)$ disappears after annealing with the C-cap at 1250 °C for all durations studied herein (1.5 h, 2.5 h and 6.6 h). The overlapping level labeled ON0b in Fig. 1 has a similar thermal activation, but different activation energy and capture cross-section parameters than $Z_{1/2}$ [25] (see also capture cross-section measurements in Appendix C). Note that there may still be some carbon vacancies present in the sample after C-cap annealing but they have been reduced to below the DLTS detection limit, i.e., $\ll 1 \times 10^{11}$ cm^{-3}. This effect is attributed to annihilation between V_C and injected C_i.

After C-injection, trap levels are appearing at 0.39 eV, 0.58 eV, 0.69 eV, 0.89 eV and 1.15 eV below E_C (see Fig. 1 and Table 1). The former three correspond to the $E_{0.38}$, $E_{0.59}$ and $E_{0.7}$ peaks, respectively, that were reported in Ref. [25]. We assign the deeper levels to the ON0a ($E_C - 0.58$ eV), ON0b ($E_C - 0.68$ eV), ON1 ($E_C - 0.89$ eV) and ON2 ($E_C - 1.15$ eV) defects observed by Okuda et al. in Ref. [24] after thermal oxidation at 1300 °C for 5 h (see also Table 1). The labeling of $E_{0.38}$ is adopted from Ref. [25] for the trap level observed at $E_C - 0.39$ eV for consistency. It should be noted here that the ON2 peak is only shown for downwards DLTS runs in Fig. 1. This is not because ON2 is not present immediately after the C-cap anneals, but rather because of noise in the upwards DLTS spectra that prevented detection of defect levels above ~400 K.

Notably, we observe (by comparison to literature, see Ref. [24]) that C-injection via both thermal oxidation and C-cap annealing causes the formation of similar trap levels. The ON-family of defect levels has been speculated to arise from carbon and/or oxygen related defects [24]. The results presented in Fig. 1 establish that the ON-levels must be related to carbon, and not oxygen, due to the negligible involvement of oxygen in our experiments. Interestingly, however, the relative intensities of the ON-peaks are different when comparing the C-cap treatments performed herein and the thermal oxidation used in Ref. [24]. After thermal oxidation, the ON1 peak was around twice as large as ON2 [24]. The 1.5 h C-injection treatment results in a similar relation, however, ON1 and ON2 are of comparable intensities after 6.6 h C-injection by carbon cap anneal (see Fig. 1b). Furthermore, ON0b was only observed after thermal oxidation followed by post-oxidation annealing in Ar at 1550 °C for 30 min in Ref. [24], in contrast to the direct appearance of the ON0b level after C-injection by C-cap anneal at 1250 °C for both 1.5 h and 6.6 h herein (see Fig. 1). Evidently, the kinetics of defect formation during C-injection strongly depend on both annealing environment (i.e., rich or poor in carbon and oxygen) and annealing duration.

DLTS measurements to ~600 K are invariably accompanied by the possibility of reverse-bias annealing of defect species. Fig. 1 demonstrates the impact of C-injection before (blue curves) and after (red

Table 1

Majority carrier trap parameters determined from the DLTS measurements in Fig. 1 including the trap labeling, energy level (E_T) with respect to the conduction band edge (E_C), apparent electron capture cross-section ($\sigma_{n,app}$), and defect assignment with corresponding references. The analysis was performed for the as-grown sample and after 6.6 h C-injection.

Label	$E_C - E_T$ (eV)	$\sigma_{n,app}$ (cm^2)	Assignment	Ref.
$E_{0.38}$	0.39	9.2×10^{-15}	C-related, $E_{0.38}$	[25]
R1	0.41	4.3×10^{-16}	S1?	[28]
ON0a	0.58	5.1×10^{-15}	C-related, $E_{0.59}$	[24,25]
$Z_{1/2}$	0.68	1.4×10^{-14}	$V_C(0/2-)$	[7]
ON0b	0.69	1.6×10^{-14}	C-related, $E_{0.7}$	[24,25]
ON1	0.89	2.6×10^{-14}	C-related	[24]
ON2	1.15	1.2×10^{-15}	C-related	[24]

curves) reverse bias annealing up to 600 K and at −5 V during the DLTS measurement (as-grown sample in black). The annealing treatment imposed by consecutive DLTS runs causes the $E_{0.38}$ level to disappear, corroborating the hypothesis that it originates from an unstable defect such as a single C interstitial [25]. The split-C_i in 4H-SiC was, in fact, recently predicted to exhibit a (2-/-) acceptor transition level at $E_C - 0.4$ eV [30], in good agreement with the $E_{0.38}$ level (see Table 1). However, the calculations in Ref. [30] also predicted another acceptor transition $C_i(0/-)$ at $E_C - 0.76$ eV which should exhibit the same thermal characteristics and most likely appear in consort with the (2-/-) level. The split-C_i was therefore assigned to the M-center in Ref. [30], a bistable defect that can exist in several different configurations and with thermal behavior matching well an unstable defect species such as an interstitial [31,32]. However, a second temperature-unstable defect level in addition to $E_{0.38}$ was not observed in the present work. Therefore, we speculate that the $E_{0.38}$ peak shown in Fig. 1 and Ref. [25] is related to C_i in a different configuration than that studied in Ref. [30].

Detailed isothermal DLTS analysis was performed in the form of Laplace-DLTS and capture cross-section measurements. The $E_{0.38}$ level was found by Laplace-DLTS to comprise of two sublevels, at $E_C - 0.33$ eV and $E_C - 0.39$ eV, indicating the involvement of two closely spaced defect levels such as C_i at hexagonal (h) and pseudo-cubic (k) lattice sites in 4H-SiC. However, capture cross-section measurements reveal a difference by a factor 20 in $\sigma_{n,app}$ between the two sublevels of $E_{0.38}$. This indicates that they may not be originating from the same point defect in two different configurations, but rather two close-lying charge transition levels. See the Appendix for further discussion, methodology and figures for Laplace-DLTS and capture cross-section measurements.

The ON-family of defect levels exhibits substantially higher thermal stabilities than $E_{0.38}$ as evidenced by their continued presence even after multiple DLTS runs to 600 K. Hence, they likely originate from more complex carbon related defects such as clusters of two or more carbon atoms. Previous theoretical studies [33–35] have reported on the aggregation of carbon interstitials in silicon carbide, a process which becomes feasible upon annealing at high temperatures. For example, Ref. [34] predicted that the carbon di-interstitial $(C_i)_2$ is electrically active in multiple configurations, where, e.g., $(C_i)_2$ in the ring-structure exhibits three charge transition levels at $E_V + 1.2$ eV (donor), $E_V + 2.0$ eV (donor) and $E_V + 2.7$ eV (acceptor). Other C related defects that could be expected to form under the experimental conditions studied in this work are clusters of 2, 3, 4, 5 or more C atoms sitting either interstitially in the lattice, on a C site as a split interstitial, or substitutionally on a Si site forming an antisite cluster. Further theoretical and experimental studies are needed to identify the microscopic structure of the defects responsible for the $E_{0.38}$ level and the ON-family of deep level defects.

3.2. Minority carrier traps

Minority carrier transient spectroscopy (MCTS) was performed to probe the defect energy levels in the lower half of the band gap before and after C-injection by C-cap annealing. The minority carrier traps
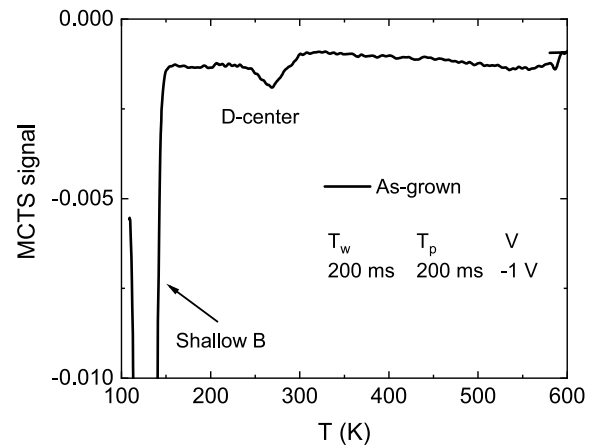

Fig. 2. MCTS spectrum for the as-grown sample using parameters T_w = 200 ms, t_p = 200 ms and V_r = −1 V.

present in as-grown material are shown in Fig. 2. Two peaks are observed and labeled B and D. The shallow boron peak (B) has been assigned to a B impurity on the Si site, B_{Si} [36]. The D-center is a deep level related to boron, but its microscopic identity has been debated, with the main candidates being a complex between B_{Si} and the V_C [37–40], and B on the C site (B_C) [21,41,42]. Recently, the assignment of the D-center to B_C was strengthened by density functional theory (DFT) calculations [22].

Fig. 3(a) demonstrates the effect of C-injection on the defect levels in the lower part of the 4H-SiC band gap after annealing with a C-cap for 1.5 h. The 200 K–500 K portion of the spectrum exhibits no discernible features indicating that no traps are formed with energy levels in the lower half of the band gap, or they are in low concentrations below the MCTS detection limit. The most intriguing features in Fig. 3(a) are related to the boron impurity. Firstly, the intensity of the shallow boron peak is reduced substantially after the C-injection treatment. Secondly, the D-center is no longer distinguishable from the background after C-injection for 1.5 h and has completely disappeared upon reverse bias annealing up to 600 K during the first MCTS run. One can here speculate that the injected C is reacting with substitutional boron, resulting in a reduction of intensity for the deep and shallow B-related defect levels observed by MCTS. A possible additional by-product of this process would be the creation of boron–carbon complexes that could introduce additional defect levels in the SiC band gap.

The MCTS spectra in Fig. 3(b) illustrate the formation of minority carrier traps after the C-cap anneal for a longer duration of 6.6 h. Again, the shallow boron peak is substantially reduced in intensity after the C-injection and two MCTS runs, but to a lesser extent than for the shorter 1.5 h C-injection treatment. Noisy MCTS spectra prevent assessment of the B-peak intensity after the first two MCTS runs. Interestingly, the longer annealing time (6.6 h) results in the formation of multiple deep levels in the lower portion of the 4H-SiC band gap that are potentially C-related and labeled T1, T2 and T3. The trap parameters for the defects probed by MCTS (shown in Figs. 2 and 3) are summarized in Table 2. Parameter extraction for the broad T3 peak was performed by fitting of the MCTS spectrum as Arrhenius analysis was not feasible. T3 likely consists of multiple close-lying defect levels but only one parameter set (the central peak) is reported in Table 2.

The two peaks at $E_V + 0.46$ eV (T1) and $E_V + 0.56$ eV (T2) (see Fig. 3b) initially have near-identical intensities which may indicate a shared origin related to the same defect center. Intriguingly, T1 and T2 are substantially enhanced after the first upwards MCTS measurement, i.e., annealing at 600 K, but are later reduced again upon a follow-up run, indicating an instability or that the responsible defects are
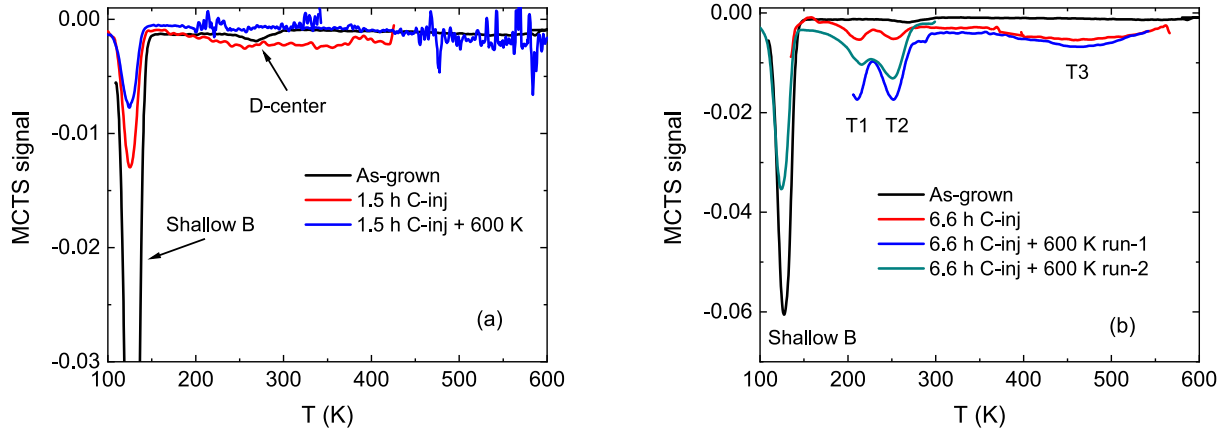
Fig. 3. MCTS spectra showing the effect of C-injection after (a) 1.5 h and (b) 6.6 h annealing with a C-cap at $1250\,°C$. The MCTS parameters for all samples were $T_w = 200$ ms, $t_p = 200$ ms and $V_r = -1$ V.

Table 2

Minority carrier trap parameters determined from the MCTS measurements including the trap labeling, energy level (E_T) with respect to the valence band edge (E_V), the apparent hole capture cross-section ($\sigma_{p,app}$), and the defect assignment with corresponding references. Parameters of B-related traps were evaluated for the as-grown sample, while parameters for traps induced by C-injection were evaluated for the 6.6 h annealed sample that was exposed to 600 K during DLTS/MCTS measurement.

Label	$E_V + E_T$ (eV)	$\sigma_{p,app}$ (cm^2)	Assignment	Ref.
Shallow B	0.27	9.4×10^{-15}	B_{Si}	[36]
D-center	0.61	1.2×10^{-14}	B_C	[22]
T1	0.46	3.0×10^{-15}	C-related	
T2	0.56	4.0×10^{-15}	C-related	
T3	1.17	4.7×10^{-14}	C-related	

Table 3

Trap concentration N_T (cm^{-3}) after the different processing steps (as-grown, annealing with a C-cap and reverse-bias annealing at 600 K during DLTS/MCTS measurement). If the trap concentration is below the DLTS/MCTS detection limit ($\ll 1 \times 10^{11}$ cm^{-3}) and we could not detect a peak signature, this is marked by 'x'. The tag 'NM' stands for 'Not measured' and means that concentration determination was difficult due to noise in the spectra.

Trap label	As-grown	1.5 h	1.5 h + 600 K	6.6 h	6.6 h + 600 K
$E_{0.38}$	x	1.3×10^{12}	x	2.3×10^{13}	x
R_1	1.9×10^{11}	x	x	x	x
ON0a	x	1.1×10^{12}	1.1×10^{12}	1.1×10^{12}	1.4×10^{12}
$Z_{1/2}$	2.1×10^{11}	x	x	x	x
ON0b	x	5.4×10^{11}	3.8×10^{11}	6.0×10^{11}	5.3×10^{11}
ON1	x	4.8×10^{11}	4.7×10^{11}	7.5×10^{11}	7.0×10^{11}
ON2	x	NM	1.9×10^{11}	NM	7.4×10^{11}
B	7.1×10^{12}	1.9×10^{12}	9.6×10^{11}	NM	4.0×10^{12}
D	2.2×10^{11}	x	x	x	x
T1	x	x	x	6.7×10^{11}	2.0×10^{12}
T2	x	x	x	6.1×10^{11}	2.2×10^{12}
T3	x	x	x	7.4×10^{11}	6.7×10^{11}

prone to reconfiguration. Furthermore, the intensity balance between T1 and T2 becomes slightly skewed after the second round of reverse bias annealing during the MCTS/DLTS runs, which may be explained, e.g., by a reconstruction of a defect complex to a different configuration. The increase in the T1 and T2 peak intensities after the first exposure to 600 K could be related to the simultaneous disappearance of the $E_{0.38}$ DLTS peak (see Fig. 1). As T1 and T2 are not visible after C-injection for 1.5 h despite the substantial reduction of the shallow B peak intensity, boron is likely not involved in their origin. The T1 and T2 levels could instead be caused by a larger carbon related cluster such as the C antisite ring structure, $(C_3)_{Si}$, which was predicted to have a defect level at about $E_V + 0.4$ eV [35] and could potentially have several configurations with different energy levels.

3.3. Evolution of trap densities with annealing

The trap concentrations of the different defects observed by DLTS and MCTS after the different processing steps are listed in the upper and lower portions of Table 3, respectively. The concentrations of the ON0a and ON0b defect levels observed by DLTS (Fig. 1) do not depend on C-injection time, while $E_{0.38}$, ON1 and ON2 all increase in density after the longer-time anneal. An independence of concentration on annealing time could indicate that defect formation is limited by the availability of one of the reactants. Furthermore, the ON-related levels exhibit only small variations with the 600 K anneal during the DLTS measurements, as opposed to the abrupt disappearance of $E_{0.38}$ after exposure to temperatures above RT.

After C-injection, both the R_1, $Z_{1/2}$ and D-levels are reduced to below the DLTS/MCTS detection limit. Interestingly, the shallow B-peak concentration is reduced by $\sim 5 \times 10^{12}$ cm^{-3} for 1.5 h C-cap annealing and by $\sim 3 \times 10^{12}$ cm^{-3} after the 6.6 h heat treatment. Out-annealing of boron impurities by diffusion is unlikely in 4H-SiC for a low temperature annealing treatment at $1250\,°C$. Therefore, as mentioned above,

a possible pathway for reduction of B-peak intensity is complex formation between B_{Si} and B_C with mobile species such as C_i. We note that the appearance of the new trap levels in the ON- and T-families does not seem to be able to account for the full reduction in B-peak concentration from the as-grown to the post-C-injection case.

3.4. Impact of C-injection on minority carrier lifetime

The annealing process outlined above has two consequences: (i) the reduction in intensity of growth-induced defects ($Z_{1/2}$, B and D), and (ii) the appearance of electrically active defect levels ($E_{0.38}$, ON-family, T1–T3) that are likely carbon related. In principle, a lower density of minority lifetime killing defects like $Z_{1/2}$ [5,6] and the D-center [23] would be expected to contribute to enhanced minority carrier lifetime. However, the new defect levels that appear as a result of the C-injection could have the opposite effect. To clarify this issue, we have performed depth-resolved TRPL measurements that provide direct insight into carrier lifetime distribution across the epi-layer after C-injection. The typical TRPL transients obtained at different depths below the surface of the as-grown sample are exemplified in Fig. 4. Note the nonlinear (non-exponential) character of the PL decay times in the near-surface region caused by carrier diffusion and surface recombination processes. In view of that, multi-component time parameters, fast (τ_1), slow (τ_2) and asymptotic (τ_3), are often introduced to describe complex carrier dynamics typical to epi-layer/substrate structures. In the present experiments, the peak photo-generated carrier density of $< 1 \times 10^{14}$ cm^{-3} is below the background doping, thus TRPL measurements are conducted
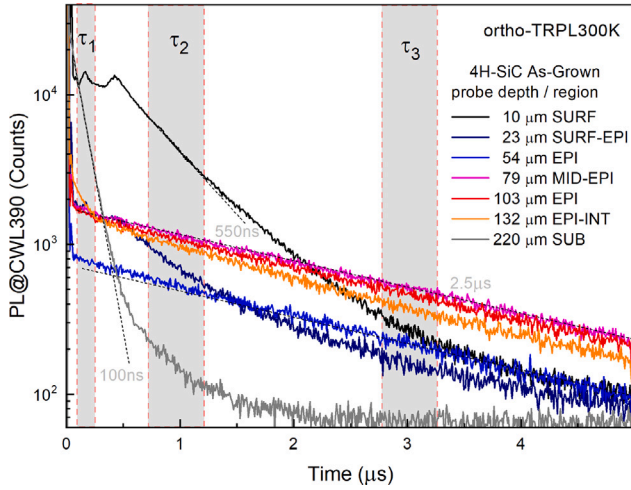
Fig. 4. Time-resolved photoluminescence (TRPL) transients obtained at different depths from the surface of the as-grown sample. The shaded areas mark the designated regions for the analysis of three decay time parameters: fast (τ_1), slow (τ_2) and asymptotic (τ_3). In the following, the C-injected samples are analyzed referring to τ_3 as the minority carrier lifetime.

under low-level injection conditions yielding the minority carrier lifetimes [43]. The analysis presented below refers to the asymptotic (τ_3) time parameter as a representative of the minority carrier lifetime, whereas the fast (τ_1) component describes the carrier lifetime in the substrate.

Fig. 5 presents the carrier lifetime profiles in the epi-layers subjected to variable duration high-temperature treatment promoting the C-injection. As expected, the carrier lifetime is smaller towards the surface due to surface recombination, and increases towards the epilayer bulk. Interestingly, for the as-grown sample (black curve in Fig. 5a), there is a maximum minority carrier lifetime of ~2.4 µs at around 80 µm depth. Thereafter, the carrier lifetime decreases as we move towards the highly doped and defect-rich substrate, where the carrier lifetime reaches a minimum value of ~100 ns for the entire epi-layer/substrate stack. This shows that the substrate contributes to reducing the minority carrier lifetime also in the bulk of the epi-layer.

One can notice from the comparison of depth-profiles in Fig. 5(a) and thermal evolutions in Fig. 5(b) that initially, after 1.5 h and 2.5 h annealing at 1250 °C, the lifetime parameters gradually decrease throughout the entire epi-layer and then, after the prolonged 6.6 h annealing, fully recover and even surpass the as-grown material in the sub-surface region (down to ~50 µm). The long duration required for the recovery is consistent with earlier reports on the necessity of prolonged thermal treatment (e.g., 3 h at 1500 °C [15]) due to slow in-diffusion process of the injected C_i that annihilate with V_C lifetime-killer centers. On the other hand, the initial deterioration of the lifetime after 1.5 h and 2.5 h anneals is unexpected and rather surprising considering the rapidity and the extensive range of this effect, i.e., significant lifetime reduction occurs already after short 1.5 h annealing and affects the entire epi-layer. It is unlikely that interstitial C can penetrate through the 150 µm thick epi-layer for such short annealing times at 1250 °C, hence the overall reduction of carrier lifetime likely results from the high-temperature treatment itself. In this regard, the most likely reason is alteration of surface recombination velocity (SRV) in the course of high-temperature treatment with a variety of potentially contributing factors, such as residual surface roughness after C-cap removal, native (spurious) SiO_2 top-layer with associated interface defect states (D_{it}), desorption of species, etc., which may affect band-bending and thus carrier leakage (recombination) at the surface. Indeed, SRV has proven as a significant lifetime limiting factor even for ultra-thick (≥ 100 µm) epitaxial layers [27,44]. This is because the measured effective lifetime

τ_{eff} is dependent on both bulk (τ_b) and surface (τ_s) recombination parameters, $\tau_{eff}^{-1} = \tau_s^{-1} + \tau_b^{-1}$, where $\tau_s \approx \frac{d^2}{\pi^2 D} + \frac{d}{2S}$ [45] with D denoting carrier diffusivity, d is epilayer thickness and S is surface recombination velocity. Under low-injection conditions, the bulk lifetime and diffusivity parameters are represented by those of the minority carriers, i.e., holes. Considering the typical reported SRV values of the order $S = 10^3$ cm/s [44,46,47], minority-hole diffusivity $D_h = 2.8$ cm^2/s [48] and lifetime τ_h in the µs-range, the diffusion length for holes $L_h = (D_h \tau_h)^{1/2}$ may well reach 50 µm, whereas the surface recombination parameter τ_s turns out to be in the same µs-range as the bulk component, both factors substantiating the importance of surface conditions. Furthermore, it is also worth noting that a substantial decline of the lifetime occurs after the high-temperature treatments (all durations) in the region close to the interface with substrate. A reaction path where defects from the substrate migrate into the epi-layer during the anneal and interact with the charge carriers cannot be excluded.

C-injection for 6.6 h results in an increase in minority carrier lifetime of ~10–20% in the top ~50 µm of the epi-layer as compared to the as-grown case (see Fig. 5). Although the maximum carrier lifetime (at ~80 µm) is not enhanced in the 6.6 h annealed sample, the affected region (0 µm–50 µm depth) is of utmost importance in, e.g., 4H-SiC power MOSFETs. A possible explanation for this increase is that injected C_i from the C-cap annihilate with V_C and cause the removal or reconfiguration of the D-center, leading to an enhancement of the carrier lifetime. To determine whether the interstitial carbon that is injected from the C-cap can penetrate SiC material until 50 µm depth, the following assumptions are made to tentatively estimate the projected diffusion length of C_i in 4H-SiC:

- No transient diffusion.
- A fundamental migration mechanism of atomic hops so the diffusivity is given by $D = D_0 \exp(-E_m/(kT))$, where E_m is the migration barrier, k the Boltzmann constant and T the temperature.
- An exponential pre-factor for diffusion of $D_0 \approx 0.01$ cm^2 s^{-1} [49].
- C_i is in the negative or neutral charge state and hence follows an activation energy for migration of 1.8 eV–2.2 eV [30].
- The diffusion length $l = \sqrt{D\tau}$ where τ is the annealing time.

Following these steps (and using $E_A = 2.1$ eV), the diffusion lengths for C_i upon annealing at 1250 °C for 1.5, 2.5 and 6.6 h become 25 µm, 32 µm and 52 µm, respectively. This agrees well with the measured range of lifetime enhancement after the 6.6 h C-cap anneal (see Fig. 5a), but contradicts the findings of Ref. [25], where the combined migration and injection barrier from the C-cap was estimated at 2.5 eV–2.8 eV based on the spatial extension of the $E_{0.38}$ peak in DLTS, which would result in the $E_{0.38}$ defect only penetrating around ~11 µm into the epi-layer according to the above considerations. However, other configurations of interstitial C may exist that are not observed using capacitance spectroscopy. In conclusion, we tentatively attribute the increase in minority carrier lifetime in the upper region of the epi-layer after 6.6 h C-cap annealing to injected C_i interacting with and diminishing the impact of lifetime-limiting defects such as $Z_{1/2}$ and the D-center.

4. Concluding remarks

We study the impact of annealing 4H-SiC samples in a carbon rich environment on material properties and formation of electrically active defects. Moderate temperature heat treatments of SiC with a C-cap result in both the reduced concentration of notable defect levels, and the appearance of new ones. The $Z_{1/2}$ and D-center defects, with previously observed detrimental impact on minority carrier lifetime in n-type 4H-SiC, are found herein to be reduced to below the DLTS and MCTS detection limits upon annealing with a C-cap at 1250 °C for 1.5 h and 6.6 h. At the same time, the concentration of the shallow boron peak as detected by MCTS (assigned to B_{Si}) is reduced by up to a factor of two depending on the annealing time. This is tentatively attributed to
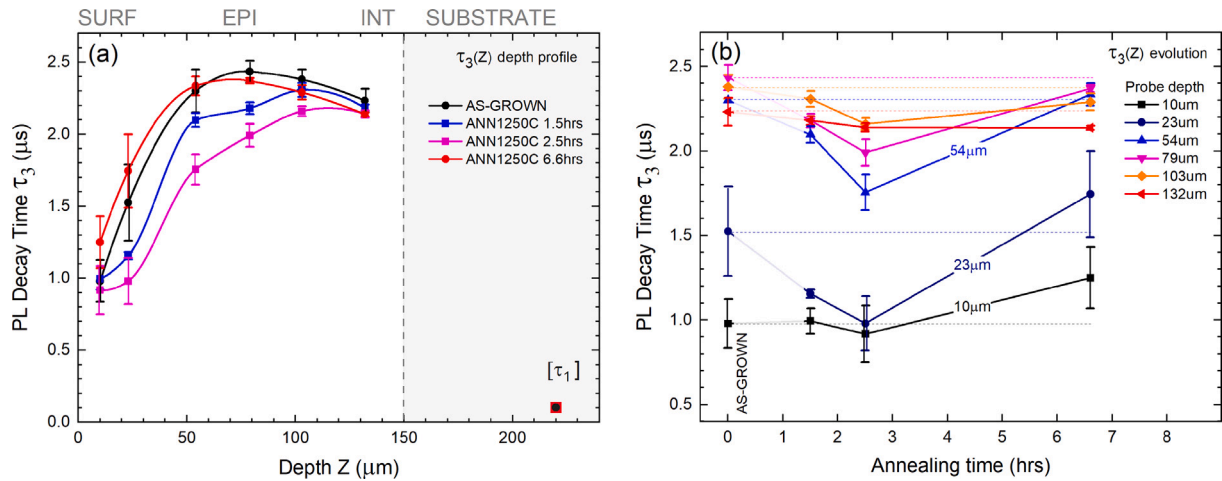
Fig. 5. Depth-resolved carrier lifetimes obtained by TRPL using decay time parameter τ_3 for analysis (see Fig. 4): (a) cross-sectional carrier lifetime profiles upon different thermal treatment, and (b) evolution of carrier lifetime at different depths from the surface with annealing time. The error bars represent the variation in repeated measurements at different probing locations of the same sample, i.e. designate the upper and lower limits of the extracted time parameters, whereas the solid lines are the guides for the eye.

interaction with injected mobile carbon species, likely single C_i, either by annihilation or complex formation.

The removal of carrier traps like the $Z_{1/2}$ and D-center is expected to affect the minority carrier lifetime. Herein, we show that the moderate temperature C-injection treatment at $1250\,°C$ can reduce or increase the minority carrier lifetime depending on the injection time. For the longer-time anneal of 6.6 h duration, the minority carrier lifetime is increased by 1020% in the top ~50 μm of the epi-layer. Further work is needed to determine whether the V_C- or B-related defect levels have the most prominent impact on the minority carrier lifetime in 4H-SiC epi-layers.

CRediT authorship contribution statement

Marianne Etzelmüller Bathen: Conceptualization, Investigation, Formal analysis, Writing – original draft, Visualization, Validation, Project administration, Funding acquisition, Supervision. **Robert Karsthof:** Conceptualization, Investigation, Formal Analysis, Visualization, Validation, Writing – original draft. **Augustinas Galeckas:** Investigation, Methodology, Formal analysis, Validation, Visualization, Writing – original draft. **Piyush Kumar:** Investigation, Formal analysis, Visualization, Writing – review & editing. **Andrej Yu. Kuznetsov:** Conceptualization, Funding acquisition, Supervision. **Ulrike Grossner:** Conceptualization, Resources, Writing – review & editing, Funding acquisition, Supervision. **Lasse Vines:** Conceptualization, Resources, Writing – review & editing, Funding acquisition, Supervision.

Declaration of competing interest

The authors declare that they have no known competing financial interests or personal relationships that could have appeared to influence the work reported in this paper.

Data availability

Data will be made available on request.

Acknowledgments

Appendix A. Isothermal DLTS measurements

Isothermal DLTS measurements to extract variations in the DLTS signal as a function of pulse width were performed using a Boonton-7200 high-precision capacitance meter operating at a test frequency of 1 MHz in combination with an Agilent 81110 A pulse generator. For direct measurements of the electron capture cross-section of a defect level, the samples were kept under a reverse bias of $-20\,V$, and forward pulses of height 20 V and of increasing length from 10 ns until 500 ms were applied. The resulting transients were evaluated with the lock-in (GS2) correlation function [50] and a window length of 640 ms. Laplace-DLTS was performed in the same setup and by keeping the sample at a fixed temperature within $\pm20\,mK$, applying a reverse bias of $-20\,V$ and forward pulses of 20 V. The resulting capacitance transients were collected for 5 s, containing 3×10^4 samples in total. 300 transients were recorded per temperature and averaged over to obtain higher signal-to-noise ratios. The emission rate spectrum was then calculated from the averaged transient based on the CONTIN algorithm [51].

Appendix B. Laplace-DLTS on $E_{0.38}$

In Fig. A.1, Laplace-DLTS spectra collected in a narrow temperature range between 160 K–168 K are shown, where emission from the $E_{0.38}$ levels occurs. The transients are revealed to contain emission from two closely-spaced levels with activation energies of $0.33\,eV$ and $0.39\,eV$, respectively. In the further course of the paper, for the purpose of clarity and consistency with our previous report [25], we will still keep the labeling to $E_{0.38}$ for the level at $E_C-0.39\,eV$, and $E_{0.38}'$ for the level at $E_C-0.33\,eV$.

The area under a peak observed in Laplace-DLTS is a measure of the corresponding trap concentration. In this case, the ratio of areas for the two levels is approximately 2:1, similar to the concentration ratio determined from simulation of conventional DLTS spectra (closer to 3:1). Such a ratio could signify the participation of two closely-spaced defect levels, e.g., the C_i at hexagonal (*h*) and pseudo-cubic (*k*) lattice sites. No such splitting was found using Laplace-DLTS for the M1 peak of the M-center [52], and the splitting between C_i(-/2-) predicted in Ref. [30] is much larger (~0.2 eV) than that found between $E_{0.38}$ and $E_{0.38}'$ herein (~0.06 eV, see Fig. A.1). Again, if $E_{0.38}$ originates from C_i, it is likely in a different configuration than the split-C_i studied in Ref. [30].
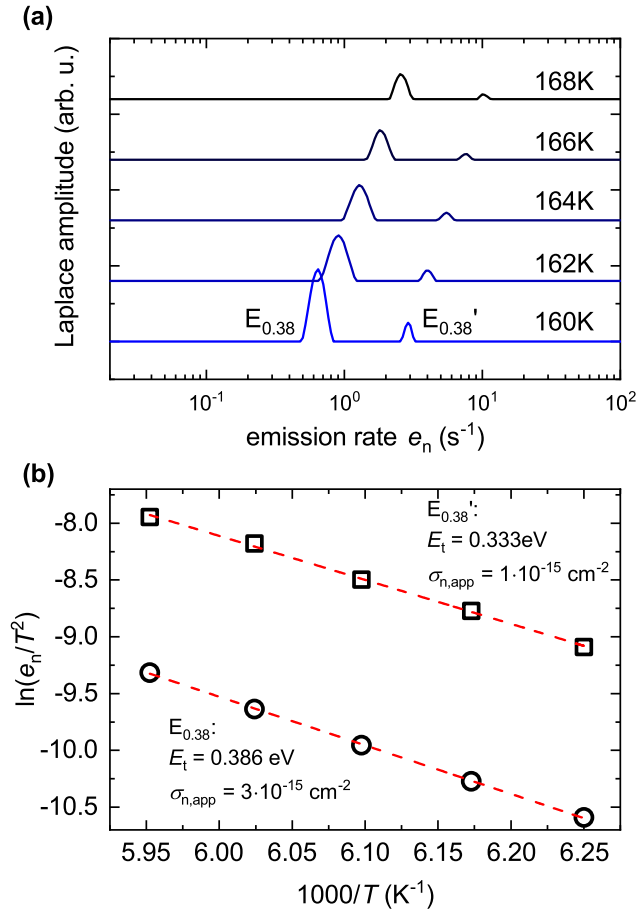
Fig. A.1. (a) Laplace-DLTS spectra of the $E_{0.38}$ level observed by DLTS in the 6.6 h annealed sample. The $E_{0.38}$ peak is shown to comprise of two sublevels. (b) The activation energies and apparent capture cross-sections of the $E_{0.38}$ and $E_{0.38'}$ sublevels are evaluated from the Arrhenius plot of their reduced emission rates.

Appendix C. Capture cross-section measurements

The capture cross-sections evaluated from Arrhenius analysis of DLTS spectra can be inaccurate, instead necessitating isothermal DLTS measurements around the peak levels. Herein, such analyses are performed for three of the trap levels: $E_{0.38}/E_{0.38'}$, ON0a and ON0b.

For the evaluation of the DLTS amplitude dependence on filling pulse length, $S(t_p)$, the following relation [53] was used:

$$S(t_p) = S(\infty) \cdot \frac{c_n}{c_n + e_n} \left(1 - \exp\left[-(c_n + e_n)t_p \right] \right), \qquad (A.1)$$

where $S(\infty)$ is the DLTS amplitude for complete trap filling, c_n is the electron capture rate, and e_n the emission rate ($e_n = 3.828\,\text{s}^{-1}$ is fixed by choice of rate window). Eq. (A.1) neglects effects of carrier capture in the transition region (the λ region). The capture cross-sections were determined from the capture rates c_n via

$$c_n = n\sigma_n \langle v_n \rangle, \qquad (A.2)$$

where n is the carrier density (determined from CV measurements) and $\langle v_n \rangle \approx 1.25 \times 10^6\,\text{cm s}^{-1}\,\text{K}^{-0.5} \times \sqrt{T}$ the thermal electron velocity [54]. The measured dependence $S(t_p)$ for the four traps $E_{0.38}$, $E_{0.38'}$, ON0a and ON0b are displayed in Fig. A.2. Note that carrier capture for the traps $E_{0.38}/E_{0.38'}$, which emit at nearly the same temperature, is visible in the measurement taken at 170 K, albeit at different filling pulse lengths. In this case, fitting was done by using a sum of two terms of the form of Eq. (A.1), with one summand for each level. Besides the concentration N_T of the respective trap, the prefactor $S(\infty)$ depends on
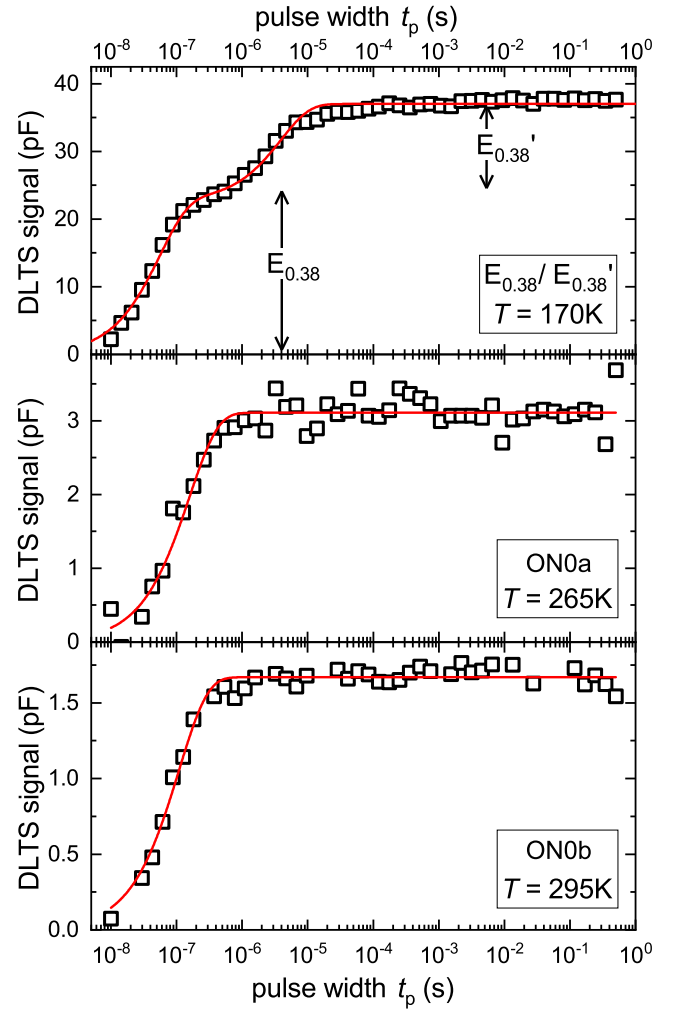
Fig. A.2. Capture cross-section measurements for the three majority carrier traps observed by DLTS below room temperature in the 6.6 h annealed sample. Fits to the data are according to Eq. (A.1).

Table A.1
Electron capture cross-sections for the four traps observed by conventional DLTS below room temperature in the 6.6 h annealed sample, as determined from the fits in Fig. A.2. Apparent capture cross-sections $\sigma_{n,app}$ from Laplace-DLTS ($E_{0.38'}$ and $E_{0.38}$) and DLTFS (ON0a and ON0b) measurements are included as well.

trap	$E_{0.38'}$	$E_{0.38}$	ON0a	ON0b
σ_n (cm^2)	5.9×10^{-17}	4.2×10^{-15}	1.5×10^{-15}	2.2×10^{-15}
$\sigma_{n,app}$ (cm^2)	1.0×10^{-15}	3.0×10^{-15}	5.0×10^{-15}	1.6×10^{-14}

the width of the region in which the trap is being filled, which is very similar for $E_{0.38}$ and $E_{0.38'}$ because of their similar activation energies. The difference in $S(\infty)$ for these two levels therefore originates from their difference in concentration. Because $E_{0.38'}$ has been determined to have only half the concentration of $E_{0.38}$, the slower capture process (with approximately 50% amplitude $S(\infty)$ compared to the fast capture process), and consequently the smaller capture cross-section, can be attributed to $E_{0.38'}$.

Table A.1 summarizes the measured capture cross-sections for the four levels ($E_{0.38}$, $E_{0.38'}$, ON0a and ON0b), along with the apparent capture cross-sections determined from Laplace-DLTS and conventional DLTS measurements. It is interesting to note that while the apparent (determined by Laplace-DLTS) and real capture cross-sections of $E_{0.38}$ are very similar, $\sigma_{n,app}$ of $E_{0.38'}$ is 20 times that of σ_n. Evaluation using conventional DLTS (lock-in) instead of Laplace-DLTS or DLTFS yielded

$\sigma_{n,app}$ =4.4 × 10^{-15} cm^2 for E$_{0.38}$' — almost two orders of magnitude larger than σ_n. This indicates that E$_{0.38}$' and E$_{0.38}$ are not originating from the same point defect in two different configurations, but rather two closely-lying charge transition levels $(q|q \pm 1)$ and $(q \pm 1|q \pm 2)$. However, this is in contradiction to the concentration difference between the two levels, prompting the speculation that we are, in fact, probing a negative-U transition of one defect. The capture cross-sections being lower for the level closer to the conduction band edge (E$_{0.38}$') points towards acceptor-like behavior, i.e., $(q|q-1)$ for E$_{0.38}$ and $(q-1|q-2)$ for E$_{0.38}$'. This is also consistent with the observation of a drop in capacitance (i.e., lower carrier density) below ∼170 K and for long C-injection times (data not shown). Here, the levels are in a more negative charge state than at room temperature, which can only lead to lower electron concentration when the levels in question are charge-compensating, i.e., acceptor-like.

References

[1] T. Kimoto, J.A. Cooper, Fundamentals of Silicon Carbide Technology: Growth, Characterization, Devices and Applications, Wiley, 2014.

[2] N. Iwamoto, B.G. Svensson, Chapter ten - point defects in silicon carbide, in: L. Romano, V. Privitera, C. Jagadish (Eds.), Defects in Semiconductors, in: Semiconductors and Semimetals, vol. 91, Elsevier, 2015, pp. 369–407.

[3] S. Castelletto, B.C. Johnson, V. Ivády, N. Stavrias, T. Umeda, A. Gali, T. Ohshima, A silicon carbide room-temperature single-photon source, Nature Mater. 13 (2014) 151–156.

[4] D.J. Christle, A.L. Falk, P. Andrich, P.V. Klimov, J. Ul Hassan, N.T. Son, E. Janzén, T. Ohshima, D.D. Awschalom, Isolated electron spins in silicon carbide with millisecond coherence times, Nature Mater. 14 (2015) 160–163.

[5] P.B. Klein, B.V. Shanabrook, S.W. Huh, A.Y. Polyakov, M. Skowronski, J.J. Sumakeris, M.J. O'Loughlin, Lifetime-limiting defects in n- 4H-SiC epilayers, Appl. Phys. Lett. 88 (2006) 052110.

[6] K. Danno, D. Nakamura, T. Kimoto, Investigation of carrier lifetime in 4H-SiC epilayers and lifetime control by electron irradiation, Appl. Phys. Lett. 90 (2007) 202109.

[7] N.T. Son, X.T. Trinh, L.S. Løvlie, B.G. Svensson, K. Kawahara, J. Suda, T. Kimoto, T. Umeda, J. Isoya, T. Makino, T. Ohshima, E. Janzén, Negative-U system of carbon vacancy in 4H-SiC, Phys. Rev. Lett. 109 (2012) 187603.

[8] H.M. Ayedh, V. Bobal, R. Nipoti, A. Hallén, B.G. Svensson, Formation of carbon vacancy in 4H silicon carbide during high-temperature processing, J. Appl. Phys. 115 (2014) 012005.

[9] T. Hornos, A. Gali, B.G. Svensson, Large-scale electronic structure calculations of vacancies in 4H-SiC using the Heyd-Scuseria-Ernzerhof screened hybrid density functional, Mater. Sci. Forum 679–680 (2011) 261–264.

[10] J. Coutinho, V.J.B. Torres, K. Demmouche, S. Öberg, Theory of the carbon vacancy in 4H-SiC: Crystal field and pseudo-Jahn-Teller effects, Phys. Rev. B 96 (2017) 174105.

[11] B. Zippelius, J. Suda, T. Kimoto, High temperature annealing of n-type 4H-SiC: Impact on intrinsic defects and carrier lifetime, J. Appl. Phys. 111 (2012) 033515.

[12] L. Storasta, H. Tsuchida, T. Miyazawa, T. Ohshima, Enhanced annealing of the Z$_{1/2}$ defect in 4H-SiC epilayers, J. Appl. Phys. 103 (2008) 013705.

[13] T. Hiyoshi, T. Kimoto, Reduction of deep levels and improvement of carrier lifetime in n-type 4H-SiC by thermal oxidation, Appl. Phys. Express 2 (2009) 041101.

[14] T. Hiyoshi, T. Kimoto, Elimination of the major deep levels in n- and p-type 4H-SiC by two-step thermal treatment, Appl. Phys. Express 2 (2009) 091101.

[15] H.M. Ayedh, R. Nipoti, A. Hallén, B.G. Svensson, Elimination of carbon vacancies in 4H-SiC employing thermodynamic equilibrium conditions at moderate temperatures, Appl. Phys. Lett. 107 (2015) 252102.

[16] Y. Negoro, K. Katsumoto, T. Kimoto, H. Matsunami, Electronic behaviors of high-dose phosphorus-ion implanted 4H-SiC (0001), J. Appl. Phys. 96 (2004) 224–228, http://dx.doi.org/10.1063/1.1756213.

[17] S.G. Sundaresan, N.A. Mahadik, S.B. Qadri, J.A. Schreifels, Y.-L. Tian, Q. Zhang, E. Gomar-Nadal, M.V. Rao, Ultra-low resistivity Al$^+$ implanted 4H-SiC obtained by microwave annealing and a protective graphite cap, Solid-State Electron. 52 (2008) 140–145.

[18] R. Nipoti, F. Mancarella, F. Moscatelli, R. Rizzoli, S. Zampolli, M. Ferri, Carbon-cap for ohmic contacts on ion-implanted 4H–SiC, Electrochem. Solid-State Lett. 13 (2010) H432.

[19] J. Zhang, L. Storasta, J.P. Bergman, N.T. Son, E. Janzén, Electrically active defects in n-type 4H–silicon carbide grown in a vertical hot-wall reactor, J. Appl. Phys. 93 (2003) 4708–4714.

[20] T. Troffer, M. Schadt, T. Frank, H. Itoh, G. Pensl, J. Heindl, H.P. Strunk, M. Maier, Doping of SiC by implantation of boron and aluminum, physica status solidi (a) 162 (1997) 277–298.

[21] I. Capan, Y. Yamazaki, Y. Oki, T. Brodar, T. Makino, T. Ohshima, Minority carrier trap in n-type 4H-SiC schottky barrier diodes, Crystals 9 (2019) http://dx.doi.org/10.3390/cryst9070328.

[22] V.J.B. Torres, I. Capan, J. Coutinho, Theory of shallow and deep boron defects in 4H-SiC, Phys. Rev. B 106 (2022) 224112.

[23] M. Ghezellou, P. Kumar, M.E. Bathen, R. Karsthof, E.Ö. Sveinbjörnsson, U. Grossner, J.P. Bergman, L. Vines, J. Ul-Hassan, The role of boron related defects in limiting charge carrier lifetime in 4H-SiC epitaxial layers, APL Mater. 11 (2023) 031107, http://dx.doi.org/10.1063/5.0142415, https://pubs.aip.org/aip/apm/article-pdf/doi/10.1063/5.0142415/16785176/031107_1_online.pdf.

[24] T. Okuda, G. Alfieri, T. Kimoto, J. Suda, Oxidation-induced majority and minority carrier traps in n- and p-type 4H-SiC, Appl. Phys. Express 8 (2015) 111301.

[25] R. Karsthof, M.E. Bathen, A. Kuznetsov, L. Vines, Formation of carbon interstitial-related defect levels by thermal injection of carbon into n-type 4H-SiC, J. Appl. Phys. 131 (2022) 035702.

[26] S. Weiss, R. Kassing, Deep Level Transient Fourier Spectroscopy (DLTFS)—A technique for the analysis of deep level properties, Solid-State Electron. 31 (1988) 1733–1742.

[27] A. Galeckas, R. Karsthof, K. Gana, A. Kok, M.E. Bathen, L. Vines, A. Kuznetsov, Cross-sectional carrier lifetime profiling and deep level monitoring in silicon carbide films exhibiting variable carbon vacancy concentrations, Phys. Status Solidi (a) 220 (2023) 2200449.

[28] M.L. David, G. Alfieri, E.M. Monakhov, A. Hallén, C. Blanchard, B.G. Svensson, J.F. Barbot, Electrically active defects in irradiated 4H-SiC, J. Appl. Phys. 95 (2004) 4728–4733.

[29] M.E. Bathen, A. Galeckas, J. Müting, H.M. Ayedh, U. Grossner, J. Coutinho, Y.K. Frodason, L. Vines, Electrical charge state identification and control for the silicon vacancy in 4H-SiC, npj Quantum Inf. 5 (2019) 111.

[30] J. Coutinho, J.D. Gouveia, T. Makino, T. Ohshima, Ž. Pastuović, L. Bakrač, T. Brodar, I. Capan, M center in 4H-SiC is a carbon self-interstitial, Phys. Rev. B 103 (2021) L180102.

[31] H.K. Nielsen, D. Martin, P. Lévêque, A. Hallén, B. Svensson, Annealing study of a bistable defect in proton-implanted n-type 4H-SiC, Physica B 340–342 (2003) 743–747.

[32] H.K. Nielsen, A. Hallén, B.G. Svensson, Capacitance transient study of the metastable M center in n-type 4H−SiC, Phys. Rev. B 72 (2005) 085208.

[33] A. Gali, P. Deák, P. Ordejón, N.T. Son, E. Janzén, W.J. Choyke, Aggregation of carbon interstitials in silicon carbide: A theoretical study, Phys. Rev. B 68 (2003) 125201.

[34] A. Gali, N.T. Son, E. Janzén, Electrical characterization of metastable carbon clusters in SiC: A theoretical study, Phys. Rev. B 73 (2006) 033204.

[35] A. Mattausch, M. Bockstedte, O. Pankratov, Carbon antisite clusters in SiC: A possible pathway to the D$_{ii}$ center, Phys. Rev. B 69 (2004) 045322.

[36] J. Zhang, L. Storasta, J.P. Bergman, N.T. Son, E. Janzén, Electrically active defects in n-type 4H–silicon carbide grown in a vertical hot-wall reactor, J. Appl. Phys. 93 (2003) 4708–4714, http://dx.doi.org/10.1063/1.1543240.

[37] S.G. Sridhara, L.L. Clemen, R.P. Devaty, W.J. Choyke, D.J. Larkin, H.S. Kong, T. Troffer, G. Pensl, Photoluminescence and transport studies of boron in 4H-SiC, J. Appl. Phys. 83 (1998) 7909–7919, http://dx.doi.org/10.1063/1.367970.

[38] A.v. Duijn-Arnold, T. Ikoma, O.G. Poluektov, P.G. Baranov, E.N. Mokhov, J. Schmidt, Electronic structure of the deep boron acceptor in boron-doped 6H-SiC, Phys. Rev. B 57 (1998) 1607–1619.

[39] P. Baranov, I. Il'in, E. Mokhov, Electron paramagnetic resonance of deep boron acceptors in 4H-SiC and 3C-SiC crystals, Phys. Solid State 40 (1998) 31–34.

[40] K. Kawahara, J. Suda, T. Kimoto, Deep levels generated by thermal oxidation in p-type 4H-SiC, J. Appl. Phys. 113 (2013) 033705.

[41] M. Bockstedte, A. Mattausch, O. Pankratov, Boron in SiC: Structure and kinetics, in: Silicon Carbide and Related Materials 2000, in: Materials Science Forum, vol. 353, Trans Tech Publications Ltd, 2001, pp. 447–450.

[42] I. Capan, T. Brodar, Y. Yamazaki, Y. Oki, T. Ohshima, Y. Chiba, Y. Hijikata, L. Snoj, V. Radulović, Influence of neutron radiation on majority and minority carrier traps in n-type 4H-SiC, Nucl. Instrum. Methods Phys. Res. B 478 (2020) 224–228.

[43] P.B. Klein, Carrier lifetime measurement in n- 4H-SiC epilayers, J. Appl. Phys. 103 (2008) 033702.

[44] T. Kimoto, H. Niwa, T. Okuda, E. Saito, Y. Zhao, S. Asada, J. Suda, Carrier lifetime and breakdown phenomena in SiC power device material, J. Phys. D: Appl. Phys. 51 (2018) 363001.

[45] A.B. Sproul, Dimensionless solution of the equation describing the effect of surface recombination on carrier decay in semiconductors, J. Appl. Phys. 76 (1994) 2851–2854, https://pubs.aip.org/aip/jap/article-pdf/76/5/2851/18669580/2851_1_online.pdf.

[46] A. Galeckas, J. Linnros, M. Frischholz, V. Grivickas, Optical characterization of excess carrier lifetime and surface recombination in 4H/6H–SiC, Appl. Phys. Lett. 79 (2001) 365–367.

[47] M. Kato, A. Ogawa, L. Han, T. Kato, Surface recombination velocities for 4H–SiC: Dependence of excited carrier concentration and surface passivation, Mater. Sci. Semicond. Process. 170 (2024) 107980.

[48] P. Grivickas, J. Linnros, V. Grivickas, Carrier diffusion characterization in epitaxial 4H–SiC, J. Mater. Res. 16 (2001) 524–528.

[49] J. Philibert, Atom Movements: Diffusion and Mass Transport in Solids, in: Monographies de Physique, Editions de Physique, 1991.

[50] A.A. Istratov, New correlation procedure for the improvement of resolution of deep level transient spectroscopy of semiconductors, J. Appl. Phys. 82 (1997) 2965–2968.

[51] S.W. Provencher, A constrained regularization method for inverting data represented by linear algebraic or integral equations, 27, 213–227.

[52] T. Knezevic, A. Hadzipasic, T. Ohshima, T. Makino, I. Capan, M-center in low-energy electron irradiated 4H-SiC, Appl. Phys. Lett. 120 (2022) 252101, http://dx.doi.org/10.1063/5.0095827.

[53] P. Blood, J. Orton, The Electrical Characterization of Semiconductors: Majority Carriers and Electron States, Academic Press.

[54] N.T. Son, W.M. Chen, O. Kordina, A.O. Konstantinov, B. Monemar, E. Janzén, D.M. Hofman, D. Volm, M. Drechsler, B.K. Meyer, Electron effective masses in 4H SiC, Appl. Phys. Lett. 66 (1995) 1074–1076.